# Distant positioning of proteasomal proteolysis relative to actively transcribed genes

Andrea Scharf[1], Petar N. Grozdanov[2], Roman Veith[3], Ulrich Kubitscheck[3], U. Thomas Meier[2] and Anna von Mikecz[1],*

[1]IUF - Leibniz Research Institute for Environmental Medicine at Heinrich-Heine University Duesseldorf, D-40225 Duesseldorf, Germany, [2]Department of Anatomy and Structural Biology, Albert Einstein College of Medicine, Bronx, NY 10461, USA and [3]Institute for Physical and Theoretical Chemistry, Rheinische Friedrich Wilhelms University Bonn, D-53115 Bonn, Germany

## ABSTRACT

**While it is widely acknowledged that the ubiquitin–proteasome system plays an important role in transcription, little is known concerning the mechanistic basis, in particular the spatial organization of proteasome-dependent proteolysis at the transcription site. Here, we show that proteasomal activity and tetraubiquitinated proteins concentrate to nucleoplasmic microenvironments in the euchromatin. Such proteolytic domains are immobile and distinctly positioned in relation to transcriptional processes. Analysis of gene arrays and early genes in *Caenorhabditis elegans* embryos reveals that proteasomes and proteasomal activity are distantly located relative to transcriptionally active genes. In contrast, transcriptional inhibition generally induces local overlap of proteolytic microdomains with components of the transcription machinery and degradation of RNA polymerase II. The results establish that spatial organization of proteasomal activity differs with respect to distinct phases of the transcription cycle in at least some genes, and thus might contribute to the plasticity of gene expression in response to environmental stimuli.**

## INTRODUCTION

The nucleus stores the genetic information for the integration of physiological signals that control proliferation and phenotypic properties of cells. Gene expression programmes are launched in the nucleus that represent end points of a great many signal transduction pathways, thus enabling cellular responses to a plethora of environmental stimuli. After the genomes of man and prevalent model organisms have been decoded, it has become increasingly clear that regulation of gene expression, e.g. the execution of different genetic programmes, requires more than the characterization of respective DNA sequences. Nuclear processes as well as their regulatory machinery are organized by a functional architecture that manifests itself in focal nuclear domains or microenvironments consisting of (ribo-) nucleic acids, proteins and dynamic complexes thereof (1–4).

Transcription constitutes the first step in gene expression. It is divided into a sequence of initiation, promoter clearance, elongation and termination. Initiation of mRNA synthesis in eukaryotes requires assembly of ∼100 protein subunits that form a scaffold of specific or general transcription factors, transcriptional co-activators, co-repressors, chromatin remodelling complexes, the mediator and the RNA polymerase II (RNAPII) holoenzyme (5–7). While the C-terminal domain (CTD) of the largest RNAPII subunit is usually hypophosphorylated during formation of the initiation complex, the transition into the elongation phase coincides with hyperphosphorylation of the CTD by kinases including subunit CDK7 (in metazoans) of general transcription factor TFIIH (8). Thus, antibodies that specifically recognize the phosphorylation state of RNAPII's CTD are used to detect respective steps of transcription, and localize initiation and elongation foci scattered throughout the nucleoplasm (9). Visualization of newly synthesized mRNA by incorporation and immediate detection of nucleotide analogues corroborates that transcriptional elongation occurs in hundreds of focal transcription factories per nucleus (10). Both, transcriptional activation and

---

elongation sites, are dynamic. Multimerization of chromosomal targets results in gene arrays that facilitate observation of 'enhanced' transcription events at a single locus. Such gene array-based techniques showed that (i) the glucocorticoid receptor (GR) activates transcription of responsive genes by transient interaction at an MMTV promoter with a residence half-time in the seconds range (11), (ii) components of the RNAPI machinery assemble on endogenous ribosomal DNA as distinct subunits and scaffolding occurs via metastable intermediates (12), (iii) assembly of the RNAPII machinery is inefficient since just 1% of polymerase-binding events result in complete transcription of mRNA (13) and (iv) some transcriptionally active chromatin is compacted more than the 30-nm chromatin fibre, and might decondense only in immediate proximity to the polymerase during transcription (14).

While regulation of gene expression occurs at all steps that lie between the synthesis of an RNA molecule and the completion of the respective protein, assembly and kinetic organisation of the transcription machinery both represent an early and major target of control. Besides integration of cell signalling pathways by co-activators, management of chromatin accessibility through epigenetic tagging, molecular switches and composition of the mediator, the ubiquitin–proteasome system represents an additional layer of transcriptional regulation in messenger RNA synthesis (15–18). It has been suggested that components of the 26S proteasome, which is made up of two flanking 19S regulatory caps and a 20S proteolytic chamber, might clear the initiation complex by freeing RNAPII, thus enabling progression into the elongation phase. Consistently, inactivation of the 19S subunit Sug1/Rpt6 results in defects of transcriptional elongation in yeast (19). However, it was likewise shown that the 19S regulatory caps of the proteasome can act independently of the 20S proteolytic particle and are recruited to the *GAL1-10* promoter by the Gal4 transactivator upon induction with galactose (20). In this context, the proteasome might not be executing its proteolytic function, but, instead, the 19S regulator/y cap might use its ATPase subunits as chaperones for non-proteolytic remodelling of protein conformations and/or interactions. In line with this, it was demonstrated that the ATPase activity of the 19S regulator has an important function in targeting the SAGA histone–acetylase complex to promoters and stimulates its interaction with transcriptional activators (21).

Besides the non-proteolytic and 20S proteasome-independent involvement of the 19S regulator in transcription processes, proteasomal protein degradation has been implicated in turnover of transcriptional activators (22–24) that might enable progression into the elongation phase by resetting the promoter (25). Genomic localization analysis and transcriptional profiling with three components of the yeast proteasome that have either regulatory or catalytic functions identified target genes including highly transcribed genes, genes controlled by mating type loci, genes involved in lipid metabolism and ribosomal protein genes (26). In these studies, similar genomic occupancies of proteasomal subunits and transcriptional activators Spt23 and Mga2 suggest concerted regulatory activity of proteasomes and their transcription factor substrates. It should be noted that proteolytic activity at the promoters was not investigated.

In addition to their role at the promoter, proteasomes have also been associated with clearance of stalled transcription machineries and transcriptional termination, since they physically associate with transcriptionally active genes at sites of DNA damage and concentrate at the 3′ ends of these genes (27). Consistent with this idea, inhibitors of proteasome-dependent protein degradation impair the recognition of termination sites.

While participation of the ubiquitin–proteasome system in transcription might be attributable to both proteolytic and non-proteolytic functions, it is unclear whether local association of proteasomal activity at a transcriptionally active gene is needed for its expression. Here, we investigated the spatial and temporal organization of two nuclear processes: proteasomal proteolysis and transcription. Using ectopic as well as endogenous gene arrays, we show that local association of proteasomes and proteasome-dependent proteolysis with the transcription machinery is not required for transcriptional initiation, elongation and protein synthesis of every gene. Consistent with this, emerging transcriptional activity in *Caenorhabditis elegans* embryos is characterized by local segregation of proteasomes and sites of transcriptional elongation. In contrast, under conditions of transcriptional inhibition substrates such as RNAPII and components of the RNA processing machinery concentrate in focal microenvironments that contain proteolytic activity.

## MATERIALS AND METHODS

### Strain maintenance, cell culture, transfection and treatments

Wild-type *C. elegans* N2 stocks were maintained at 20°C using standard methods (28). HEp-2 cells (American Tissue Culture Collection) were cultured in RPMI 1640 medium supplemented with 10% fetal bovine serum (FBS), nonessential amino acids, L-glutamine and penicillin and streptomycin (pen/strep). Murine embryonic fibroblasts (kind gift from Peter Hemmerich) were cultured in low-glucose Dulbecco's modified eagle medium (DMEM) supplemented with 10% FBS, nonessential amino acids, L-glutamine and pen/strep. E3 cells (29) were cultured in low-glucose DME containing 10% FBS. E3 cells were transiently transfected with expression plasmids using FuGene 6 (Roche) for 24–30 h according to the manufacturer's protocol. The following plasmids were used: MS2-GFP. Transcription of the transgene was induced using 6 μg/ml doxycycline overnight. Transcriptional inhibition was induced by adding AMD (1 μg/ml) or $HgCl_2$ (60 μM) for 4 h. For *in situ* localization of proteasomal protein degradation under conditions of RNA polymerase I inhibition, $HgCl_2$ (50–70 μM) and DQ-Ova were comicroinjected into the nucleus and cells were incubated between 60 and 90 min before fixation. Where indicated, cells were coincubated with 1–5 μM MG132 for 16 h to inhibit proteasomal activity.

## Antibodies

The following antibodies were used for indirect immuno-fluorescence (IF) or western blot (WB) where indicated: human anti-K48 linked polyubiquitin (Apu2.07; 30) at 1:100 (embryos) and 1:500 (human cells); human anti-K63 linked polyubiquitin (Apu3.A8; 30) at 1:500 (embryos) and 1:1000 (human cells); mouse anti-HP1$\gamma$ (2 MOD-1G6, Euromedex) at 1:4000; rabbit anti H3K9m3 (ab8898, Abcam) at 1:50; rabbit anti H3K4m3 (ab8580, Abcam) at 1:40; human serum against SmB/B′ (collected from Scleroderma patients at the Dermatology Clinic of the Heinrich-Heine-University Duesseldorf, Germany) at 1:100 (WB); mouse anti-tubulin (Tub 2.1, Sigma) at 1:1000; mouse anti-20S (MCP231, Biomol) at 1:500 (WB); rabbit anti-20S (PW8155, Biomol) at 1:20–1:100; rabbit anti-26S (kindly provided by B. Dahlmann, Berlin, Germany) at 1:50; mouse anti RNAPII (H5; Covance) at 1:50; human serum against RNAPII (kindly provided by R. Mierau, Aachen, Germany) at 1:50; human serum against CenpC (#17, were collected from Scleroderma patients at the Dermatology Clinic at Heinrich-Heine-University Duesseldorf, Germany) at 1:1000; rat anti-BrdU (OBT0030, Oxford Biotechnology) at 1:50; mouse anti-calnexin (H-70, Santa Cruz) at 1:1000; mouse anti-SC35 (sc-35, Sigma) at 1:1000; mouse anti-fibrillarin (72B9, kindly provided by M. Pollard, Scripps Research Institute, La Jolla; CA, USA) at 1:20.

Secondary antibodies (Jackson ImmunoResearch Laboratories) conjugated to FITC, rhodamine, Cy2; Cy3, or Cy5 were used at dilutions of 1:100 in IF. Secondary antibodies were used at 1:10 000 (anti-rabbit, -human) and 1:5000 (anti-mouse IgG; IgM) in WBs.

## Indirect IF and microscopy

Cells were seeded on coverslips, grown to subconfluence, fixed and permeabilized using procedures (i)–(iii):

  (i) Rinsed in phosphate-buffered saline (PBS), fixed in methanol (5 min, −20°C), permeabilized in acetone (2 min at −20°C).
 (ii) Rinsed in PBS, fixed in 4% formaldehyde (10% formaldehyde methanol free, Polysciences) in PBS [10 min, room temperature (RT)), permeabilized in 0.25% Triton X-100 (3 min; RT).
(iii) Rinsed in PBS, fixed in 4% formaldehyde in PBS (20 min, RT), washed three times with PBS, permeabilized with 1% Triton X-100 (5 min, RT).

*Caenorhabditis elegans* embryos were obtained by cutting gravid hermaphrodites, prefixation of released embryos in 4% formaldehyde for 5–40 min, freeze cracking between slide and coverslip, direct fixation in −20°C methanol for 5 min and permeabilization in −20°C acetone for 2 min. After fixation and permeabilization, cells or *C. elegans* embryos were washed in PBS and subjected to IF as described previously (31). Imaging was performed at RT using (i) a 60x/1.25 NA UPlanFl, a 60x/1.4 NA planapo or a 100x/1.4 NA planapo objective on an inverted confocal laser-scanning microscope (Fluoview IX70, Olympus) or (ii) a 63x/1.4 NA objective on a LSM 510Meta laser

scanning microscope (Zeiss). Figures were assembled in Photoshop (Adobe).

## Biochemical fractionation and chromatin isolation

Cells were grown in culture flasks and left untreated or exposed to chemicals as indicated. After the indicated times, cells were detached by trypsination. Collected cells were washed twice with PBS and then lysed in lysis buffer consisting of 0.01 M Tris–HCl pH 7.5; 0.01 M NaCl, 0.015 M MgCl$_2$ and 0.5% Triton X-100 at 4°C. After centrifugation at 2500$g$ for 10 min, the supernatant was collected as cytoplasmic fraction while the pellet was further resuspended and sonicated to obtain a complete nuclear lysate. For chromatin-isolation collected cells were washed twice in PBS and lysed in buffer A (0.01 M HEPES pH 7.6; 0.01 M KCl; 0.015 M MgCl$_2$; 0.34 M Sucrose; 10% Glycerol; 0.001 M DTT, Pefablock) for 8 min on ice. After centrifugation at 1300$g$, the supernatant was collected as cytoplasmic fraction while the pellet was washed in buffer A, resuspended in buffer B (0.003 M EDTA; 0.0002 M EGTA, 0.001 M DTT; Pefablock) and incubated for 45 min on ice. After centrifugation at 1700$g$ for 5 min, the supernatant was collected as soluble nuclear fraction and the pellet was washed in buffer B and collected as insoluble nuclear fraction/chromatin-enriched fraction. The DNA in the insoluble nuclear fraction was sheared.

## Immunoblotting

Proteins from whole cell lysates or cell fractions separated by sodium dodecyl sulphate–polyacrylamide gel electrophoresis (SDS–PAGE) were transferred to Hybond N (Amersham) and incubated with indicated antibodies in PBS containing 0.5% Tween-20 with 5% nonfat dried milk. Bound antibodies were detected using horseradish peroxidase-conjugated secondary antibodies and the ECL system (Amersham), according to the manufacturer's instructions.

## S5a-Pull down

Nuclear fractions were prepared as described above. Pellets containing nuclear fractions were resuspended in TBS containing 5% glycerol and 0.5% Triton X-100 followed by sonication. Binding was performed by incubation of the nuclear fraction with GST-S5a agarose (Biomol) overnight at 4°C. Bound proteins were washed in TBS/5% glycerol/0.5% Triton X-100 and in one last washing step without Triton X-100. Bound proteins were boiled in loading buffer, separated in a 6% SDS–PAGE and immunoblotted. 50 mM glutathione was added to the samples with GST-S5a agarose as a competitor to corroborate specificity of RNAPII binding (Figure 6C, lane GSH).

## *In vivo* immunolabelling of nascent RNA transcripts

Fluorouridine (FU) incorporation assays were performed to detect newly synthesized RNA as previously described (32,33). Cells were grown on coverslips to subconfluence. FU was added to the culture medium (0.02 M working

concentration) and coverslips were removed for fixation after 5–10 min. Subsequently, cells were fixed using 4% formaldehyde/0.25% Triton X-100 and the halogenated nucleotide was detected with a rat anti-BrdU antibody (Sigma) at 1:50.

### *In situ* localization of proteasomal proteolysis

Cells were seeded on coverslips and grown to subconfluence. For *in situ* localization of proteasomal protein degradation in subnuclear compartments DQ-ovalbumin (DQ-Ova; 0.1–0.5 mg/ml in PBS) or a combination of DQ-Ova with DQ-BSA (0.1 mg/ml in PBS) was microinjected into the nucleus. DQ-Ova and DQ-BSA are fluorogenic substrates for proteases. A strong fluorescence quenching effect is observed when proteins are heavily loaded with BODIPY dyes. Upon hydrolysis of DQ-Ova or DQ-BSA to single, dye-labelled peptides by proteases, this quenching effect is relieved, producing brightly fluorescent products. Thus, fluorescence intensity equals local proteolytic activity, and visualizes an intracellular process that can be subjected to kinetic imaging analyses. DQ-Ova and DQ-BSA fluorescence either was imaged in living cells or by cell fixation 10–60 min post injection according to protocols (i)–(iii)(see above).

### Fluorescence *in situ* hybridization

Fluorescence *in situ* hybridization (FISH) was performed as previously described (29,34). Briefly, E3 cells were grown on coverslips and induced with 6 µg/ml doxycycline overnight. Cells were rinsed in PBS, fixed in 4% formaldehyde (20 min, RT), washed twice with PBS and incubated with 70% ethanol over night at 4°C. Cells were rinsed twice in PBS and permeabilized with 0.5% Triton X-100 (10 min, RT). After washing with PBS, cells were rinsed twice in 40% formamide/2× SSC (5 min each). They were hybridized overnight at 37°C in 30 µl/coverslip of a solution containing 0.01 % RNase-free BSA, 1.5 µg single-stranded DNA (ssDNA)/tRNA, 2× SSC, 40% formamide, and 10 ng of probe. The cells were washed twice with 40% formamide/2× SSC for 15 min at 37°C and twice with PBS for 1 h. Then the cells were refixed in 4% formaldehyde for 20 min, washed in PBS and immunolabelled. Cells were mounted with Pro-Gold mounting medium. Imaging was performed as described previously (29) with a 60×/1.4 NA planapo objective on an inverted microscope (1X81; Olympus) connected to an air-cooled charge-coupled device camera (Sensicam QE; Roper Scientific) run by IPLab Spectrum software (Scanalytics).

### Quantification

Quantification analysis of fluorescence and WB was performed with Metamorph image analysis software package (MSD Analytical Technologies) or counted manually using fluoview (Olympus) or the Zeiss LSM image browser (Zeiss). Linescans were taken from contrast-enhanced blowups as indicated.

### Fluorescence recovery after photobleaching and fluorescence recovery after photobleaching analysis

Fluorescence recovery after photobleaching (FRAP) analysis was performed on a Zeiss LSM 510 Meta confocal microscope, equipped with an argon laser (488 nm and 100 mW power), and an incubation chamber with temperature control and $CO_2$ supply. Cell measurements were performed at 37°C and 5% $CO_2$ partial pressure. HEp-2 cells were grown in Matek-Dishes to subconfluence and subjected to micro-injection with 0.2 mg/ml DQ-Ova at 37°C. Cells recovered in 15 min and were detected with a 63× oil / 1.4NA objective (Zeiss). For ATP depletion, cells were cultivated post microinjection in medium with 0.01 M sodium azide and 0.05 M 2-deoxyglucose at 37°C. Two to four proteolytic foci per nucleus were selected for bleaching. Three prebleach images were taken with 20 µW/µm$^2$ (0.5% AOTF transmission). Photobleaching was performed with 2 mW/µm$^2$ (100% AOTF transmission) for 31 s. Subsequent images were taken with 20 µW/µm$^2$ (0.5% AOTF transmission) to avoid bleaching during the acquisition phase. Z-stacks were taken every 160 s to account for cell movement during the acquisition phase. Typically, each z-stack contained around 10 images. In total, eight z-stacks were taken per cell, corresponding to an observation time of ∼20 min. Image analysis was performed with ImageJ and Origin 8.0. First, unbleached foci inside the prebleach image were used to find the right image plane containing the recovery information from the z-stack. The new time stack was slightly smoothened. A region of interest (ROI) was placed manually around each bleached focus in each image. An additional ROI was placed around the whole cell for correction of potential photobleaching during the acquisition phase. To obtain normalized and bleach corrected intensity versus time plot, the data were normalized according to

$$I(t) = \frac{B(t) \cdot N_0}{N(t) \cdot B_0}$$

where $B(t)$ is the intensity of the bleached spot ROI changing with time, $B_0$ is the intensity of the bleached spot ROI in the prebleach image, $N(t)$ is the intensity of the whole cell ROI changing with time and $N_0$ is the intensity of the whole cell ROI in the prebleach image (35). The normalized data of each focus were collected and a mean normalized intensity versus time plot generated for the different experimental conditions.

### SMM

The mobility analysis of single proteolytic foci was performed on a custom-built wide-field epi-fluorescence microscope based on an Axiovert 200 microscope body (Zeiss), equipped with a highly sensitive Andor iXon DV 860-BI EMCCD camera with 128 × 128 pixels and with a Sapphire 100 DPSS-laser illumination with 488 nm (36). Single focus imaging was performed using a 63 × oil/ 1.4 NA objective (Zeiss) and ∼2 fps acquisition time at RT. Single focus tracking was performed using DiaTrack 3.03 (Semasopht). Calculation of the

mean-square-displacement was performed according to (37) with Origin 8.0 (Originlab). To obtain a diffusion coefficient the first ~10 linear points of each MSD plot were fitted with

$$\langle r^2 \rangle = 4Dt$$

where $<r^2>$ is the two-dimensional MSD, $D$ is the diffusion coefficient and $t$ the time lag.

## RESULTS

### Proteolytic microenvironments in the nucleus contain ubiquitinated proteins, degrade different substrates and are immobile

We have shown previously that proteasomal activity can be visualized in nucleoplasmic foci by microinjection of the fluorogenic precursor substrate DQ-ovalbumin (DQ-Ova) into the cell nucleus, and proteasome inhibitor-sensitive detection of its fluorescent cleavage products by confocal laser-scanning microscopy (38). To characterize such centres of proteolytic activity in more detail, different cell types were analysed with respect to nuclear localization and numbers of DQ-Ova foci. In murine embryonic fibroblasts (MEFs), human osteosarcoma cells (E3) and human epithelial cells (HEp-2) fluorescent DQ-Ova cleavage products are diffusely distributed throughout the nucleoplasm, and concentrate in 7–90 bright foci per nucleus (Figure 1A, B and D). A HEp-2 nucleus contains an average of 29 proteolytic centres. Confocal detection of simultaneously microinjected DQ-Ova (green) and the likewise quenched DQ-BSA (red) showed that both substrates are degraded in the same proteolytic microenvironments (Figure 1C, micrograph, blowups, linescan). Similar results were obtained by co-injection of DQ-Ova and the fluorogenic precursor substrate succinyl-LLVY-amino-methyl-coumarin (data not shown).

Since it is not known if DQ-Ova or DQ-BSA is tagged for proteasome-dependent degradation by poly-ubiquitin chains, it was tested if proteolytic microenvironments contain ubiquitinated substrates. To this end, microinjected DQ-Ova was double-labelled with antibodies that specifically detect tetraubiquitin chains linked via lysine (K) at position 48 or 63, respectively (30). Cleaved DQ-Ova as well as K48-tetraubiquitin and K63-tetraubiquitin are localized in a similar pattern of multiple foci throughout the nucleoplasm (Figure 1D). K63-linked tetraubiquitin additionally shows distinct staining in the cytoplasm (Supplementary Figure S1). Representative linescans and quantification of fluorescent signals in 35 nuclei show that 57% of the proteolytic centres colocalize with K48-tetraubiquitin and 60% proteolytic centres colocalize with K63-tetraubiquitin (Figure 1D, graph, right), suggesting degradation of endogenous substrates in these domains.

Nuclear processes such as replication, DNA repair, transcription and RNA maturation occur in highly dynamic microenvironments (4). To determine the mobility and dynamics of DQ-Ova degradation sites,

kinetic imaging techniques were applied. Single molecule microscopy revealed that a proteolytic centre moves in an area of $2 \times 2$ pixels within a time window of 150 s. The respective trajectory starts at pixel position 76/32 ($y$-axis/$x$-axis), and moves to pixel position 78/34 over time (Figure 1E, upper panel, right). The corresponding graph of mean-square-displacement (MSD) values over time shows a linear increase within the first 75 s, suggesting free diffusion followed by a parabolic curve progression that is probably due to a combination of free diffusion and an additional directed movement (Figure 1E, lower panel). It is important to note that the measurements were performed in a confined area of small scale, e.g. several pixels, representing conditions where the intrinsic dynamics of the cell system do matter. To account for intrinsic cell movement linear MSD-values of 46 proteolytic foci from 13 cells were used for determination of a mean diffusion coefficient of $2 \times 10^{-5}\,\mu\text{m}^2/\text{s} \pm 0.3 \times 10^{-5}\,\mu\text{m}^2/\text{s}$, suggesting that DQ-Ova degradation centres are nearly immobile.

Next, the dynamics of DQ-Ova proteolytic centres were analysed by FRAP that enables observation of the mobility of fluorescently labelled molecule populations due to their inherent photosensitivity (39). DQ-Ova was microinjected into cells, selected proteolytic foci were bleached and recovery of fluorescent signals was observed over time (Figure 1F, look up table depiction, arrows). Accumulated data from FRAP analyses of 49 DQ-Ova microenvironments show that at 37°C proteolytic foci return in a biphasic manner that is characterized by a fast increase of fluorescence in the regime of three minutes postbleach, followed by a slower recovery (Figure 1G, black curve). Under physiological conditions (37°C), fluorescence recovery reaches 16% within 17.7 mi. In ATP-depleted cells, recovery is also biphasic, but reduced, since it reaches a plateau of 11% recovery after 9 min (Figure 1G, red curve). The FRAP experiments, as presented here, suggest that recovery of fluorescent DQ-Ova cleavage products is mainly due to continuous protein degradation within proteolytic sites. This assumption is strengthened by the results of ATP depletion that, among other things, inhibits ubiquitination and proteasomal protein degradation. Consistent with an exhaustion of the protein degradation process, the normalized fluorescence intensity of proteolytic centres immediately postbleach is significantly reduced in ATP-depleted versus control cells (Figure 1H).

### Proteasomal activity locates to euchromatin

To characterize their association with chromatin, DQ-Ova foci were double-labelled with DNA dyes, heterochromatin-associated protein HP1γ and histone H3 that is trimethylated at lysine position 9 (H3K9m3). The DNA dye topro3 stains euchromatic regions with a homogeneous, transparent pattern throughout the nucleoplasm, and concentrates in bright heterochromatic areas, especially in the periphery of nucleoli (Figure 2A; third micrograph). The corresponding merged micrograph, blowup and linescan show that DQ-Ova foci are embedded in euchromatic regions, but excluded from regions with high DNA concentration that indicate
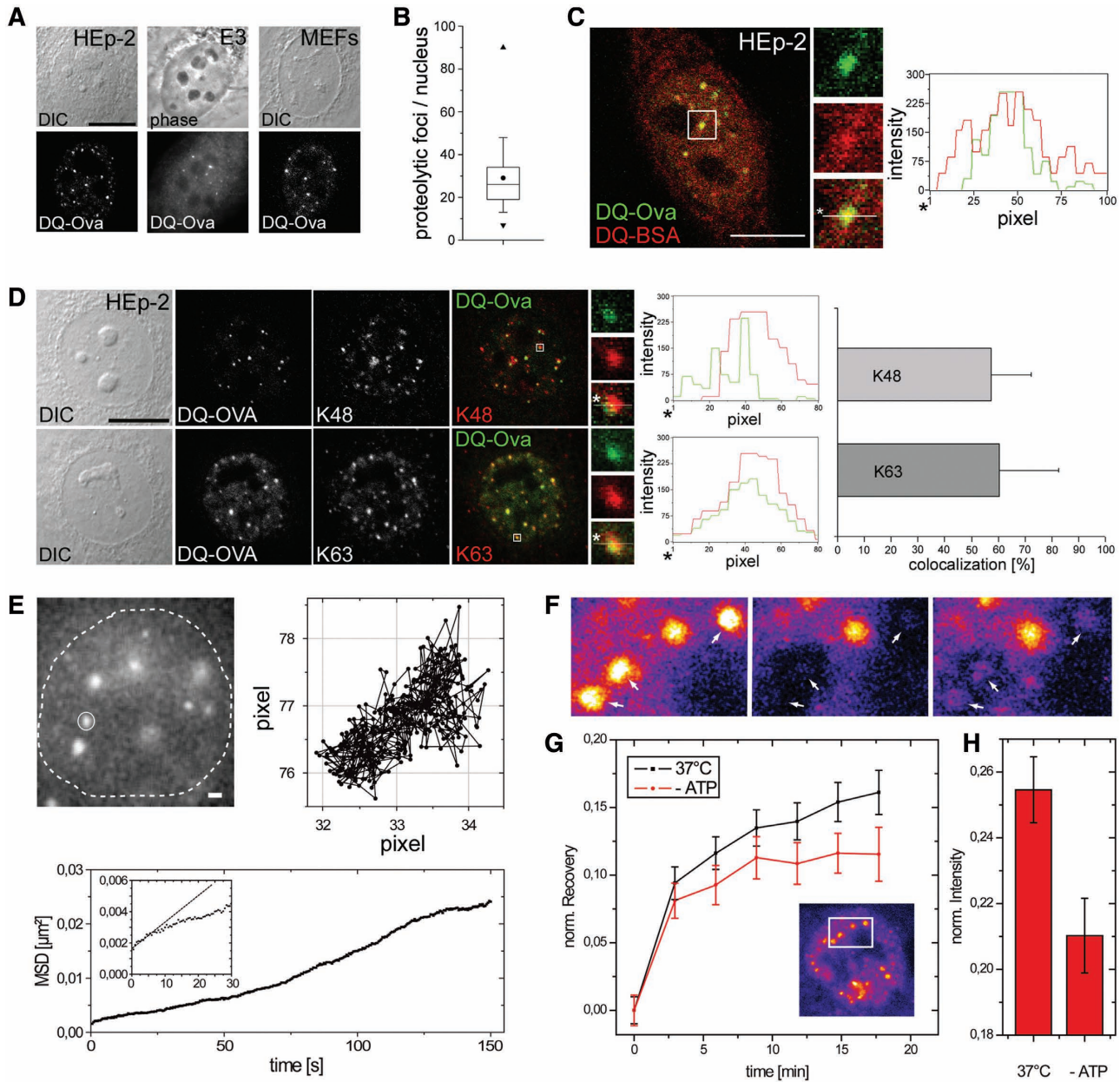
**Figure 1.** Proteasomal proteolysis in the cell nucleus is spatially confined. Proteasome-dependent protein degradation was monitored by microinjection of the fluorogenic substrate DQ-Ova into nuclei. (**A**) Subnuclear localization of DQ-Ova degradation sites was analysed by confocal fluorescence microscopy in different mammalian cell types. Bar, 5 μm. (**B**) Quantification of proteolytic foci per nucleus in HEp-2 cells. The boxplot represents data of 59 nuclei from eight independent experiments. (**C**) Comicroinjection of DQ-Ova and DQ-BSA into a HEp-2 cell nucleus shows that both substrates are degraded in the same nuclear microenvironment (merge, blowup and linescan). Bar, 5 μm. (**D**) Double labelling of DQ-Ova and antibodies against K48- or K63-linked tetraubiquitin shows that polyubiquitinated proteins are components of proteolytic microenvironments (merge, blowups and linescans). Quantification of colocalization between green and red fluorescence signals indicates that 57% of proteolytic foci overlap with K48-linked and 60% with K63-linked polyubiquitinated proteins. Values represent means ± SD from four independent experiments each ($n = 35$). Bar, 5 μm. (**E**) Proteolytic foci are nearly immobile. DQ-Ova was microinjected into a HEp-2 cell nucleus (micrograph, dotted line) and monitored with two frames/second over 200 s. The trajectory shows the position of one proteolytic focus (micrograph, continuous circle) over time. The graph (lower panel) depicts the mean square displacement (MSD) of this focus plotted against the time. The first 10 linear points of the curve were used to calculate a diffusion coefficient (inset). (**F**) Fluorescence recovery after photobleaching (FRAP) experiments were performed on HEp-2 cells that were microinjected with DQ-Ova into the nucleus. Micrographs show areas that contain proteolytic foci before the bleach pulse (pre-bleach, left), immediately after the bleach pulse (post-bleach, middle), and after 17.7 min of fluorescence recovery (right). Images represent look up tables from time-lapse FRAP data sets. Arrows label three bleach regions that contain one proteolytic focus each. (**G**) Quantification of FRAP experiments at 37°C without (37°C) or with treatment with 10 mM sodium azide/50 mM 2-deoxyglucose after microinjection (-ATP). The graph shows mean values ± SEM (bleached proteolytic foci = 49 from eight independent experiments) as relative fluorescence recovery after normalization of the post-bleach levels to zero. (**H**) The graph shows post-bleach mean values ± SEM as relative fluorescence intensity after normalization to pre-bleach levels.
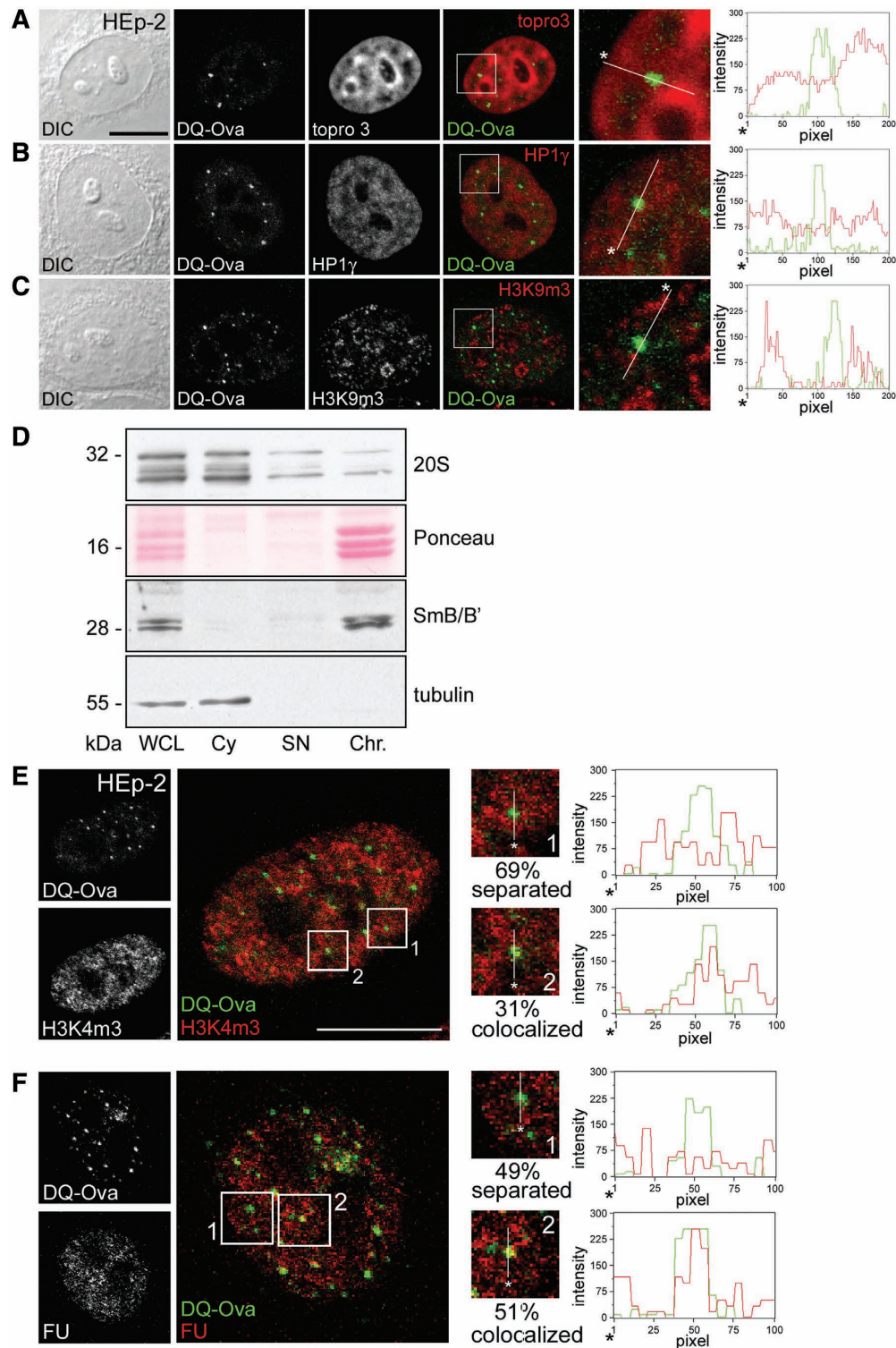
**Figure 2.** Localization of proteasomal proteolysis in euchromatin. (**A–C**) Confocal fluorescence micrographs of representative HEp-2 cells that were microinjected with DQ-Ova (green) and double-labelled (red) with TO-PRO3 (A), HP1γ (B) or H3K9m3 (C). Proteolytic foci are localized in euchromatic regions (merges, blowups, linescans). Bar, 5 μm. (**D**) HEp-2 cells were fractionated into a cytoplasmic (Cy), soluble nuclear (SN) or chromatin-enriched nuclear fraction (Chr). Protein fractions were analysed by western blot to determine the levels of 20S proteasomes or signature proteins of the fractions as control (nuclear, snRNP component SmB/B′; cytoplasm, tubulin). The enrichment of chromatin in respective fractions is monitored by the concentration of histone proteins that occur as prominent bands between 14 and 20 kDa (Ponceau). WCL, whole cell lysate. (**E**) Micrographs of a representative HEp-2 cell microinjected with DQ-Ova into the nucleus and immunostained with antibodies against H3K4m3, an epigenetic mark of transcriptionally active euchromatin. Thirty-one percent of the proteolytic foci are localized in transcriptionally active euchromatin, whereas 69% are not locally associated (merge, blowups and linescan; six independent experiments, $n = 20$). (**F**) Micrographs of a representative HEp-2 cell that was microinjected with DQ-Ova into the nucleus and subjected to fluorouridine incorporation to label sites of active transcription. After fixation, cells were immunostained with antibodies against BrdU to detect sites of FU incorporation. 51% of the proteolytic foci are colocalized with sites of active transcription, whereas 49% are separated (merge, blowups and linescan; three independent experiments, $n = 17$).

heterochromatin (Figure 2A). The exclusive localization of proteolytic microenvironments in euchromatin was corroborated by the absence of colocalization with heterochromatin markers HP1γ and H3K9m3 (Figure 2B and C; micrographs, linescans).

Proteolytic activity in euchromatic regions consequently raises the issue of association of proteasomes with chromatin. Immunoblots show that while proteasomes are predominately occurring in the cytoplasmic protein fraction, they partially cofractionate with chromatin-free nuclear fractions and, to a lesser extent, with chromatin-enriched nuclear fractions that contain histone proteins (Figure 2D; immunoblot and Ponceau stain). The colocalization and cofractionation results suggest that proteasomal proteolysis as well as proteasomes occur in nucleoplasmic microenvironments that are characterized by a low concentration of chromatin.

### Proteasomal activity partially colocalizes with global transcription

Since condensation of chromatin generally antagonizes nuclear processes, active gene expression is mostly located in euchromatin (14). Due to the localization of proteasomal activity in euchromatic regions, we next analysed the spatial relationship between sites of transcriptional and proteolytic activity in the nucleoplasm. Labelling of microinjected DQ-Ova and antibodies against histone 3 that is epigenetically marked by trimethylation at lysine position 4 (H3K4m3) during the transcription process (40,41) shows a granular distribution of H3K4m3 throughout the nucleoplasm (Figure 2E). Quantification of double-labelling experiments with DQ-Ova indicates that 31% of proteolytic foci colocalize with H3K4me3-marked chromatin, whereas the remaining 69% do not. Separation of proteolytic and transcriptional sites can be described in more detail in respective linescans that clearly show a central DQ-Ova focus (green) encased by H3K4m3 signal (Figure 2E; linescan 1, red).

In addition to the antibody-based analysis, protein degradation and transcriptional processes were observed simultaneously by DQ-Ova proteolysis and *in situ* run on assays that monitor incorporation of the nucleotide analogue fluorouridine (FU) during transcript elongation. While fluorescent degradation products of DQ-Ova concentrate in an average of 29 distinct foci, nascent RNAs are distributed in a granular nucleoplasmic pattern that is composed of hundreds of transcriptionally active microenvironments (Figure 2F, red). The Cook and Hager labs determined 1900–8000 transcription sites per human nucleus (10,42,43). Notwithstanding the abundance of transcriptionally active microenvironments, quantification showed that only 51% of proteolytic centres colocalize with nascent RNAs (Figure 2F), and only 17% colocalization was observed between proteasomes and nascent RNAs (data not shown). In line with the H3K4m3 signal-based results, simultaneous visualization of proteolysis and global transcription identifies a limited local association of these two nuclear processes that is precluded from in-depth analyses by the heterogeneity of

ongoing gene programmes due to concurrent detection of various cell cycle and transcriptional phases.

### Proteasomal activity and proteasomes are not colocalized with every induced transcription site

To examine positioning between proteasomal proteolysis and transcription in a defined gene programme, a cell system was used that exclusively visualizes single transcription sites. It is based on previously established methods that allow for observation of gene expression from the time a defined gene is induced via the levels of DNA, RNA and respective protein product in living cells (29,44). The system consists of a stable cell line with a tandem transgene array (∼50 copies) inserted into a single site. Nascent RNA is detected by FISH against a specific intron of the β-globin gene (intron 1) or by expressed MS2 bacteriophage coat protein fused to green fluorescent protein (GFP) and bound to MS2 stem–loops placed in the 3′-untranslated region (UTR) of the transcript. Additionally, the transcript encodes a cyan fluorescent protein (CFP) fusion protein that is targeted to peroxisomes when RNA processing, mRNA transport and translation are completed.

Intron 1 of β-globin RNA concentrates at the site of the gene array in a single bright spot (Figure 3B-2, -4, -6 and -8). Proteolytic products of DQ-Ova localize in a homogeneous pattern throughout the nucleoplasm, and concentrate in brighter foci. Despite the analogous distribution, proteolytic activity is excluded from the induced transcription site (Figure 3B-8). The presence of the CFP fusion protein in peroxisomal spots indicates that the entire process of gene expression has gone to completion (Figure 3B-5), and suggests that local association of proteasomal activity with the promoter/gene array is not required for transcription of the β-globin transgene.

In order to rule out the possibility that local association of proteasomal protein degradation is required at the gene array that cannot be visualized by DQ-Ova proteolysis, we next analysed the distribution of 20S proteasome core particles in correlation with transcription of fusion protein MS2-GFP (Figure 3C). MS2-GFP distributes in a smooth homogeneous pattern throughout the nucleoplasm and concentrates in a bright spot that indicates nascent MS2 transcripts, containing MS2 stem–loop RNA, at the site of the gene array (Figure 3C-2, -4, -6 and -8). 20S proteasomes locate to the cytoplasm and nucleoplasm, excluding nucleoli (Figure 3C-3). Despite their ubiquitous distribution in the nucleoplasm, 20S proteasomes do not colocalize with MS2-GFP at the induced transcription site (Figure 3C-8), indicating that recruitment of proteasomes to the respective promoter is not required for transcription of MS2 RNA. The presence of the CFP fusion protein in bright peroxisomal spots (Figure 3C-5) demonstrates that the entire process of gene expression has gone to completion without local presence of proteasomes at the gene array.

We next examined the local organization of proteasomal proteolysis and an endogenous gene array that represents a natural platform for gene expression. Ribosomal DNA (rDNA) genes are organized as
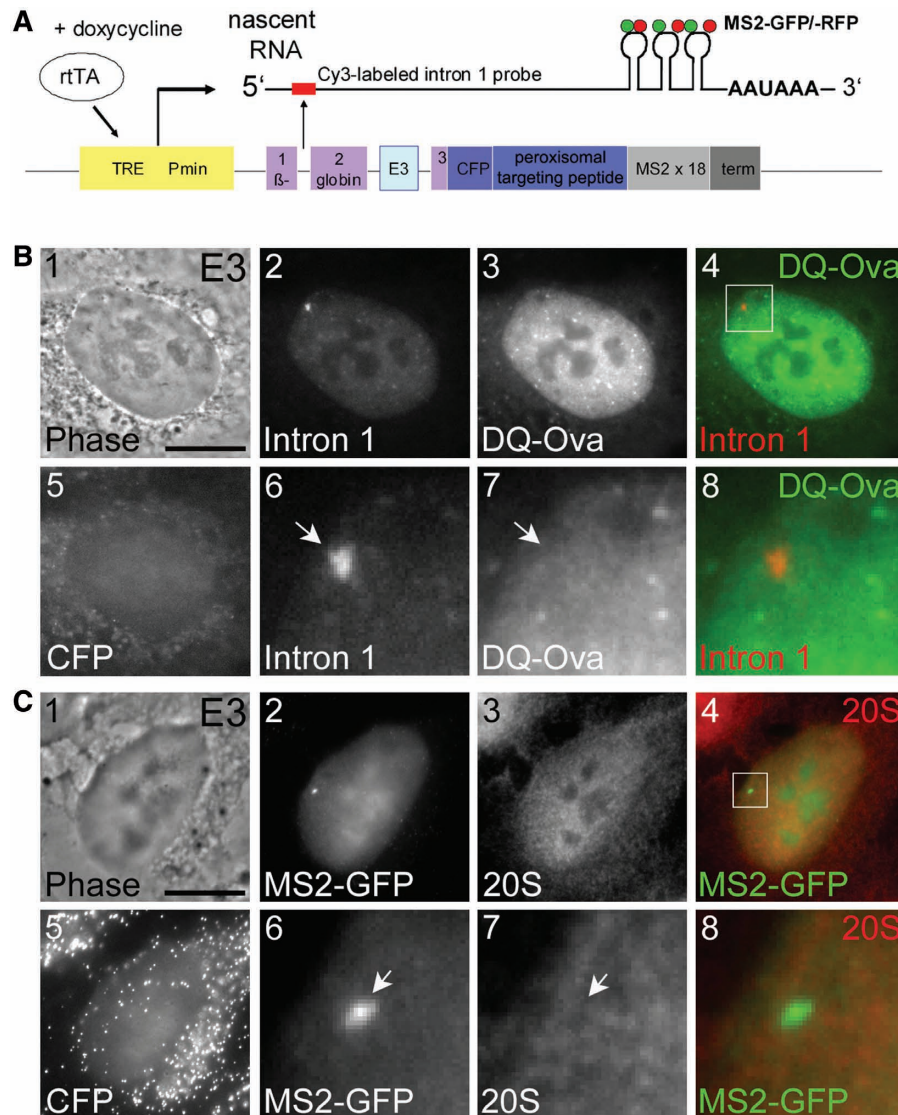
**Figure 3.** Proteasomes and proteasomal activity are not localized at induced genes/sites of transcription initiation. (A–C) Stable human U2OS cell line expressing a transgene from an inducible promoter. (A) Schematic of the construct that was stably integrated into the genome of the cell line E3. It consists of the human β-globin gene with three exons, two introns, and a short 5′ untranslated region (UTR). Exon 3 was truncated and fused in-frame to CFP containing the peroxisomal targeting tripeptide SKL at its COOH terminus; thus, functional transcription and translation induces fluorescent peroxisomes. The 3′UTR encompasses 18 MS2 stem–loop repeats, which provide tight binding sites for the MS2 coat protein when transcribed. Expression is driven by a minimal CMV promoter (Pmin) under the control of the tetracycline response element (TRE) and inducible by the presence of doxycycline (dox) by the transactivator (rtTA) (29). (B) Induced E3 cells were microinjected with DQ-Ova into the nuclei, fixed, permeabilized and assayed by FISH with Cy3-labeled probes to intron 1. The induced transcription site appeared as a bright focal signal of intron 1 (B2, blowup B6, arrow). The panels B4 and B8 depict the merge of the intron 1 signal with proteolytic microenvironments (B3, blowup B7) showing that there is no proteolytic activity at the induced transcription site. Note that (i) the intron 1 signal and DQ-Ova are pseudo-coloured, and (ii) the direct fluorescence of the β-globin-CFP in peroxisomes is weaker than in (C) due to the FISH procedure, but, nevertheless, indicates successful induction of transgene expression. (C) Fluorescent micrographs of an E3 cell that was transfected with MS2-GFP, induced for transgene expression, fixed, permeabilized and immunostained with antibodies against 20S proteasomes (C3, C7 blowup). The direct fluorescence of β-globin-CFP in peroxisomes indicates completed expression of the gene (C5), whereas the induced transcription site can be visualized by direct fluorescence via MS2-GFP (C2, blowup C6, arrow). The panels C4 and C8 depict the merge of the MS2-GFP and the 20S proteasome staining in pseudo-colour showing that proteasomes are absent from the induced transcription site.

tandem repeats in nucleolar organizer regions (NORs) that enable transcription of the huge amounts of ribosomal RNA needed for the assembly of ribosomes (45). NORs imaged in HEp-2 cells by a specific autoimmune serum (Figure 4A and D, red) or concentration of silver ions (AgNOR, Figure 4B and E, dark grey) are located predominately in nucleoli (right column, blowups, white circles) and to a lesser extent throughout the nucleoplasm.

Colocalization analysis with either 20S proteasomes (Figure 4A and B, 20S, green) or DQ-Ova (Figure 4D and E, green) by confocal microscopy shows (i) no proteasome signal in 88% of the NORs and 82% of the AgNORs (Figure 4C), and (ii) that 90% proteolytic foci occur without NOR association and 91% without AgNOR association (Figure 4F). These results suggest that neither the presence of proteasomes nor their
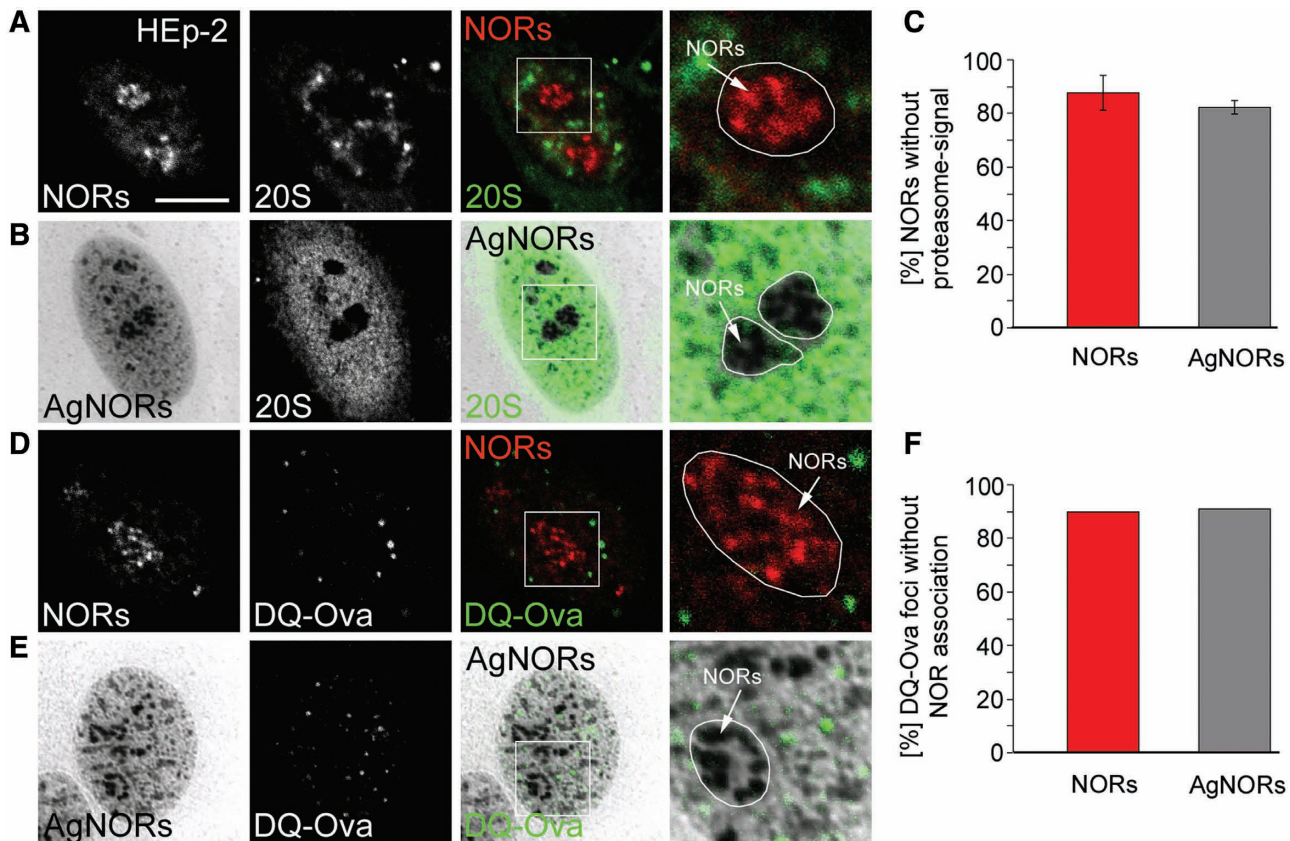
**Figure 4.** Proteasomes and proteasomal activity are not localized at sites of ribosomal RNA transcription. Endogenous gene array: ribosomal genes are labelled by a human patient serum against nucleolar organizer regions (NORs, **A,D**) or silverstaining (**B** and **E**). (A, B, D and E) Confocal fluorescence micrographs of NORs in representative HEp-2 cells double-labelled with antibodies against proteasomes (green; A and B) or micro-injected with DQ-Ova (green; D, E). Bar, 5 μm. Quantification of (**C**) NORs in relation to proteasomes from three independent experiments ($n = 300$) and (**F**) the positioning of proteolytic foci in relation to NORs from three independent experiments (NORs: $n = 19$; AgNORs: $n = 22$).

activity at NORs is required for transcription and expression of rDNA. The completeness of rDNA gene expression, e.g. rRNA biogenesis, was monitored by ribosome profiling (data not shown).

**Transcription of early genes in *C. elegans* embryos occurs without local association of proteasomes or their substrates**

We have shown that proteolytic activity is localized neither at the inducible transcription site of the human β-globin transgene array nor at endogenous rRNA gene arrays. To validate the relevance of these results *in vivo*, we analysed embryos of the nematode *C. elegans*. *Caenorhabditis elegans* embryos are primarily controlled by maternal factors; thus, the expression of the early genes during the first cell divisions represents a defined gene programme (46–48). Gravid hermaphrodites were cut and released embryos freeze-cracked, fixed and labelled with antibodies against hyperphosphorylated RNAPIIo that indicate transcriptional elongation (49). The elongating RNAPIIo-molecules are localized throughout the nucleoplasm of worm embryos in a punctuated pattern (Figure 5B–G, red). It should be noted that not all nuclei show RNAPIIo staining, because in *C. elegans* mRNA synthesis is inhibited in the

early embryonic germ lineage (49). Labelling of the ubiquitin–proteasome system in *C. elegans* embryos reveals that proteasomes are distributed in the cytoplasm and throughout the nucleoplasm in distinct foci and a diffuse localization pattern (Figure 5B, green). Proteins marked for degradation via K48-linked tetraubiquitin occur in the cytoplasm and nucleoplasm. In the nucleus, they localize within larger foci that develop to distinct microdomains in late embryonal stages (Figure 5C–G, green). Independent of the developmental stage of the embryo proteasomes and tetraubiquitinated proteins are generally not colocalized with RNAPIIo foci. Local overlap between proteasomes or K48-linked nuclear proteins with RNAPIIo-signals could only be observed in scattered nuclei (Figure 5B, F and G; blowups, arrows, yellow). Consistent with the results of the gene arrays, proteasomes and their substrates, e.g. K48-linked tetraubiquitinated proteins, are localized separately from early transcribed genes in *C. elegans*.

**Inhibition of transcription induces nuclear protein degradation centres**

The spatiotemporal analysis of proteolytic and transcriptional processes has revealed that neither proteasomes nor proteasomal degradation have to be locally associated
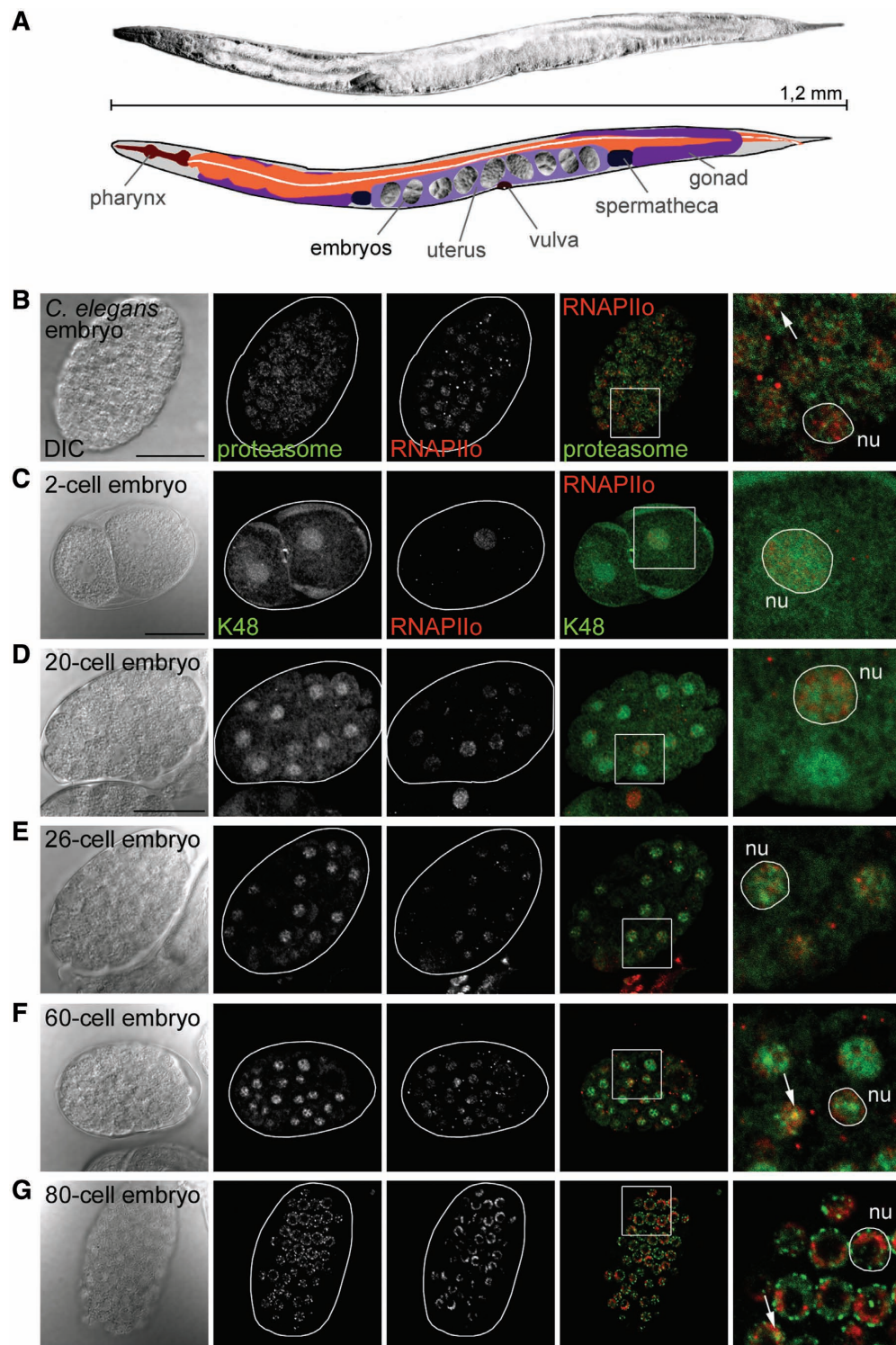
**Figure 5.** Proteasomes and tetraubiquitinated nuclear proteins are not localized at early transcribed genes in *C. elegans* embryos. (**A**) Schematic of the anatomy of a gravid *C. elegans* hermaphrodite with fertilized eggs/embryos in the uterus. (**B–G**) Confocal fluorescence micrographs of representative *C. elegans* embryos in different developmental stages double-labelled with antibodies against hyperphosphorylated RNAPIIo (red) and (B) proteasomes (green) or (C–G) K48-linked polyubiquitin (green). Neither proteasomes nor proteins, which are tagged for proteasomal degradation, are spatially associated with elongating RNAPIIo. Scattered nuclei show colocalization (right column, insets, arrows, yellow). nu, nucleus. Bar, 20 μm.

with induced gene loci during the initial steps of gene expression. However, previous results in yeast indicate a physical interaction of RNAPII/template DNA and proteasome-dependent degradation of RNAPII under conditions of stalled transcription or transcriptional termination (27). In order to explore the distribution of proteasomal activity when transcription is inhibited, DQ-Ova foci were localized in nuclei of actinomycin D (AMD)-treated cells. While the number of proteolytic microenvironments per nucleus does not change after inhibition of transcription, a subpopulation of DQ-Ova foci redistributes to enlarged rounded speckles that contain the non-snRNP splicing factor SC35 (Figure 6A, lower panel, linescan). A detailed list of rounded speckle components and confocal micrographs that show recruitment of RNAPII to these subnuclear microenvironments are available in Supplementary Data (Supplementary Table 1; Supplementary Figure S2). Inhibition of proteasomal activity by MG132 corroborates that especially the differentially phosphorylated forms of RNAPII represent substrates of proteasome-dependent protein degradation as shown by increased signal intensity between the prevalent bands representing RNAPIIo (240 kDa) and RNAPIIa (220 kDa), respectively (Figure 6B and D, third lane). Consistent with this, pull-down experiments show that hyperphosphorylated RNAPII (RNAPIIo) as well as hypophosphorylated RNAPII (RNAPIIa) interact with subunit S5a of the 19S regulator which recognizes ubiquitinated substrates (Figure 6C). The inhibition of transcription by AMD induces a destabilization of RNAPIIa that can be partially rescued by MG132 (Figure 6D). These results suggest that inhibition of transcription by the DNA intercalator AMD induces a local association of proteolytic microenvironments with rounded speckles that correlates with degradation of their protein components, e.g. RNAPII.

To strengthen the idea that transcription-off situations induce local association of proteolytic centres with nuclear proteins that are involved in gene expression, RNA polymerase I (RNAPI) was specifically inhibited with subtoxic concentrations of mercuric chloride ($HgCl_2$) as described previously (31). Incubation of HEp-2 cells with $HgCl_2$ for 4 h induces nucleoplasmic clusters containing RNAPII, 20S proteasomes and fibrillarin (Figure 6E). Fibrillarin is normally located in the nucleolus and has a role in early processing and modification of ribosomal RNA, and ribosome assembly (50). $HgCl_2$ induces the redistribution of fibrillarin into nucleoplasmic clusters and its proteasomal degradation (31). Co-microinjection of DQ-Ova and $HgCl_2$ results in increased nucleoplasmic colocalization of fibrillarin with proteolytic microenvironments/centres (Figure 6F) corroborating the idea that inhibition of RNAPI-dependent transcription induces the redistribution of fibrillarin and its degradation in the nucleoplasm (31).

## DISCUSSION

Nuclear processes such as DNA replication, DNA repair, transcription of RNAs and their processing are organized in dynamic microenvironments that are functionally connected to the ubiquitin–proteasome system via proteolytic and non-proteolytic pathways (51,52). While the importance of proteasome-dependent protein degradation for nuclear function is generally acknowledged, the investigation of local proteasomal activity in the nucleus is still in its infancy. Yet, a crucial determinant for the lifetime of a protein or protein complex is if the proteolytic machinery is within reach or positioned at a distance. Consistent with this idea, it was shown that degradation of several nuclear proteins is correlated with their subnuclear localization (31,53–56).

We recently developed an application that enables localization of proteasome-dependent proteolysis in the nucleoplasm (38,57), and show here that proteolytic microenvironments follow the paradigm of nuclear organization (1–4) since they occur as focal domains in euchromatic regions. The analysis of spatial interactions between proteolytic and transcriptional sites reveals that (i) local positioning of these two nuclear processes is variable and (ii) at least some genes do not require local proteolytic activity and the presence of proteasomes at the promoter for execution of gene expression. The absence of cleaved DQ-Ova as well as proteasomes at an induced β-globin gene array, and detection of respective gene products in the cytoplasm, indicates that all stages of gene expression such as transcriptional initiation, elongation, RNA processing, RNA transport and translation have been completed without proteasomal activity at the corresponding transcription site. These results find confirmation in observations that endogenous rDNA gene arrays are likewise not locally associated with proteasomes and proteasomal activity. Most importantly, it is shown here that embryonic transcripts in *C. elegans* are synthesized under conditions of distantly positioned proteasomes in relation to transcriptional elongation. Taken together, the results somewhat confine the model that suggests recruitment of 26S proteasomes to initiated transcription sites, and promotion of transcriptional elongation by *in situ* degradation of components of the initiation machinery (58).

Investigation of the spatial and temporal organization of proteasomal proteolysis and transcription on a global level, as we also performed, confirms that expression of genes does not always require local association of the ubiquitin–proteasome system. The idea of association patterns that depend on the different phases of the transcription cycle could integrate conflicting literature concerning the demonstration of proteasomes and proteasomal subunits at promoters (20,26,59,60). It should also be noted that all these studies were antibody based and, thus, did not particularly include analysis of proteolytic activity, as presented here. As a result, a local involvement of proteasomal protein degradation in transcriptional initiation and elongation should not generally be anticipated.

A different paradigm emerges under transcription-off conditions. Inhibition of transcription invariably induces formation of proteolytically active microenvironments in the nucleoplasm that contain components of the ubiquitin–proteasome system and the transcription machinery.
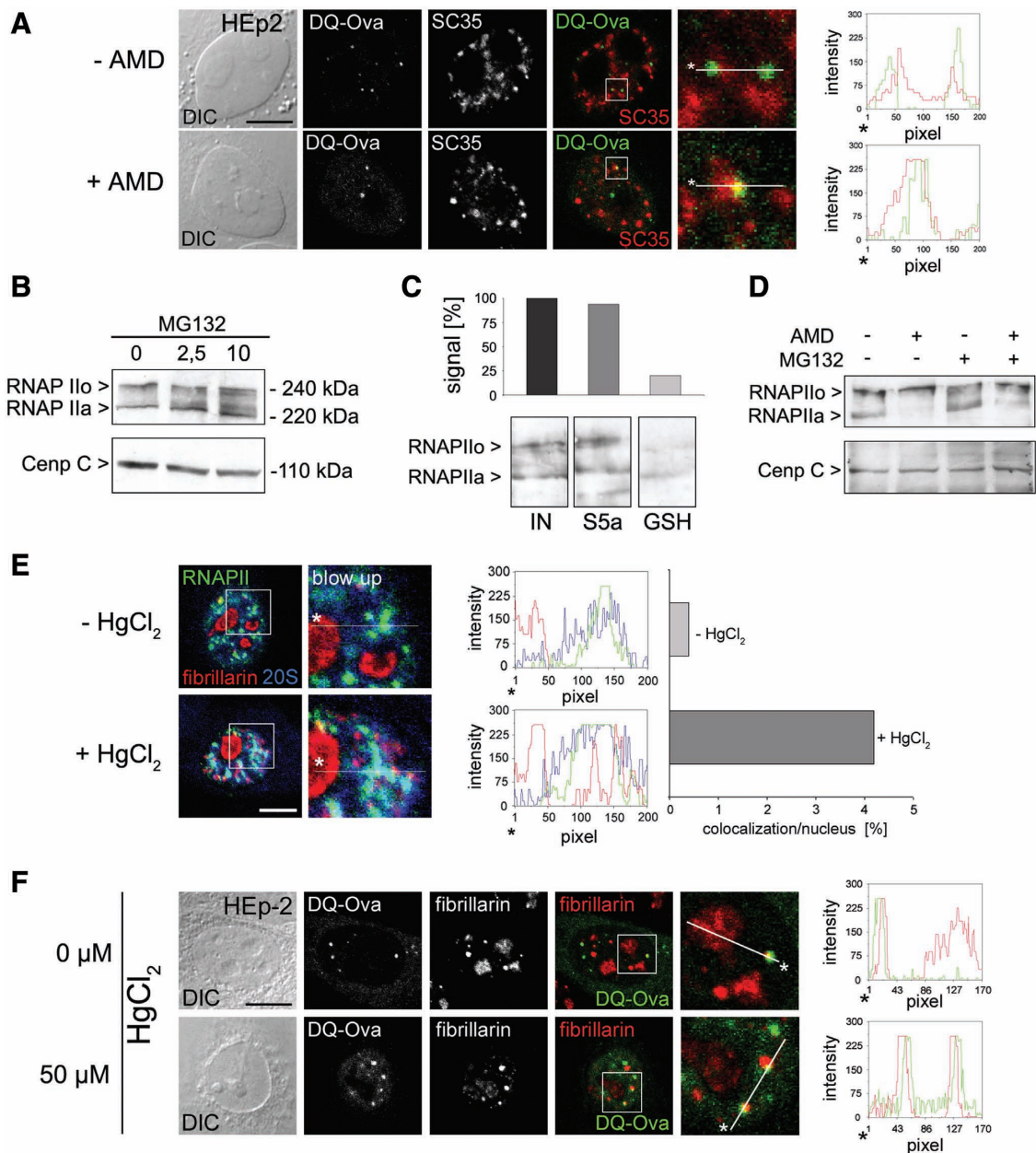
**Figure 6.** Upon transcriptional inhibition, components of the gene expression machinery cluster in proteolytic microenvironments and are degraded by proteasomes. (**A**) Double-labelling of DQ-Ova and antibodies against non-snRNP splicing factor SC35 in untreated (upper panel) or AMD-treated (4 h, lower panel). AMD-treatment induces bright rounded speckles that partially contain proteolytic activity (bottom, merge, blowup and linescan). (**B**) Whole cell lysates of HEp-2 cells treated with increasing concentrations of proteasome inhibitor MG132 for 16 h were subjected to WB to determine the levels of RNAPII, and centromere protein CENP-C (loading control). (**C**) A pull-down assay with the 19S regulator subunit S5a, followed by a WB with antibodies against RNAPII, shows physical association between S5a and RNAPII. IN, input; GSH, specificity control. (**D**) Whole cell lysates of HEp-2 cells that were left untreated or treated with 2.5 μM MG132 for 16 h or with 1 μg/ml AMD for 4 h or a combination thereof, were subjected to western blot analysis to determine the concentration of RNAPII and centromere protein CENP-C as loading control. (**E**) Confocal immunofluorescence indicates partial colocalization of fibrillarin, 20S proteasomes and RNAPII in nucleoplasmic clusters after 4 h of HgCl$_2$ treatment (+HgCl$_2$, merge, blowup, linescan). Respective quantification shows a 10-fold increase of colocalization in HgCl$_2$-treated cells. Values represent means from two independent experiments ($n = 127$). (**F**) Microinjection of DQ-Ova (upper panel) or a combination of DQ-Ova with HgCl$_2$ (lower panel) shows that a subpopulation of HgCl$_2$-induced nucleoplasmic fibrillarin clusters contain proteolytic activity (merge, blowups, linescans).

The induction of these proteolytic microenvironments is correlated with proteasome-dependent degradation of transcriptionally relevant proteins such as RNAPII. Thus, it is suggested that local concentration of proteasomal activity occurs at sites of interrupted transcription and might aid to clear the respective chromatin from the transcription complex. This idea has been put forward previously when it was shown that proteasomes physically and functionally interact with chromatin at sites of stalled transcription (27). It was

demonstrated that transcriptional arrest at DNA lesions recruits the ubiquitin ligase Nedd4 and induces ubiquitination of RNAPII (61,62). Thus, nucleoplasmic structures such as enlarged, rounded speckles (63–65) might represent junkyards that function as active protein degradation centres when nuclear processes are inhibited, and respective (ribo-) nucleoprotein complexes rendered redundant. Consistent with this, we show here for the first time that rounded speckle domains are proteolytically active.

Taken together, local concentration of proteolytic activity represents a versatile tool for regulation of gene expression. The formation of protein degradation centres seems to be co-ordinately organized with nuclear processes such as transcription that likewise occur in confined microenvironments in response to respective cellular stimuli and requirements. In line with this idea, recruitment of 20S proteasome core particles to the promoter under transcription-off conditions was demonstrated previously by shutting down the vascular endothelial growth factor (VEGF) promoter, and time-resolved chromatin immunoprecipitation (ChIP) analysis (66). An attractive hypothesis is that recruited proteasomes form a proteolytic microenvironment and degrade HIF-1 or other transcription factors at the promoter. Notably, association of the 19S regulator with the VEGF promoter remained constant underlining a 20S core particle-independent and non-proteolytic role of 19S regulatory caps in transcriptional processes (20,21,66). Since the functional architecture of the nucleus is characterized by considerable dynamics of its structures, it will be important to advance techniques that likewise enable characterization of the dynamics of proteasome-dependent proteolysis and its nuclear substrates. Kinetic imaging of proteolytic foci by single molecule microscopy and FRAP as performed in this study defines nuclear microenvironments of DQ-Ova degradation as immobile. This immobility argues against a model that proteolytic centres roam the nuclear space and scan it for potential substrates. Thus, a major topic of future investigations concerns the identification of molecular triggers that initiate and regulate local proteolytic activity. Given the distinct positioning of proteasomal proteolysis with respect to transcription sites, it will be important to elucidate if nuclear distribution patterns of protein degradation contribute to selective tuning of different gene programmes.

## SUPPLEMENTARY DATA

Supplementary Data are available at NAR Online.

## REFERENCES

1. Wansink,D.G., Schul,W., van der Kraan,I., van Steensel,B., van Driel,R. and de Jong,L. (1993) Fluorescent labeling of nascent RNA reveals transcription by RNA polymerase II in domains scattered throughout the nucleus. *J. Cell Biol.*, **122**, 283–293.
2. Stein,G.S., Zaidi,S.K., Braastad,C.D., Montecino,M., van Wijnen,A.J., Choi,J.-Y., Stein,J.L., Lian,J.B. and Javed,A. (2003) Functional architecture of the nucleus: organizing the regulatory machinery for gene expression, replication and repair. *Trends Cell Biol.*, **13**, 584–592.
3. Trinkle-Mulcahy,L. and Lamond,A.I. (2007) Toward a high-resolution view of nuclear dynamics. *Science*, **318**, 1402–1407.
4. Misteli,T. (2007) Beyond the sequence: cellular organization of genome function. *Cell*, **128**, 787–800.
5. Dvir,A., Conaway,J.W. and Conaway,R.C. (2001) Mechanism of transcription initiation and promoter escape by RNA polymerase II. *Curr. Opin. Genet. Dev.*, **11**, 209–214.
6. Kornberg,R.D. (2005) Mediator and the mechanism of transcriptional activation. *Trends Biochem. Sci.*, **30**, 235–239.
7. Clapier,C.R. and Cairns,B.R. (2009) The biology of chromatin remodelling complexes. *Annu. Rev. Biochem.*, **78**, 273–304.
8. Phatnani,H.P. and Greenleaf,A.L. (2006) Phosphorylation and functions of the RNA polymerase II CTD. *Genes Dev.*, **20**, 2922–2936.
9. Martin,S., Failla,A.V., Spöri,U., Cremer,C. and Pombo,A. (2004) Measuring the size of biological nanostructures with spatially modulated illumination microscopy. *Mol. Biol. Cell*, **15**, 2449–2455.
10. Jackson,D.A., Iborra,F.J., Manders,E.M. and Cook,P.R. (1998) Numbers and organization of RNA polymerases, nascent transcripts, and transcription units in HeLa nuclei. *Mol. Biol. Cell*, **9**, 1523–1536.
11. McNally,J.G., Muller,W.G., Walker,D., Wolford,R. and Hager,G. (2000) The glucocorticoid receptor: rapid exchange with regulatory sites in living cells. *Science*, **287**, 1262–1265.
12. Dundr,M., Hoffmann-Rohrer,U., Hu,Q., Grummt,I., Rothblum,L.I., Phair,R.D. and Misteli,T. (2002) A kinetic framework for a mammalian RNA polymerase *in vivo*. *Science*, **298**, 1623–1626.
13. Darzacq,X., Shav-Tal,Y., Phair,R.D., Shenoy,S.M. and Singer,R.H. (2007) *In vivo* dynamics of RNA polymerase II transcription. *Nat. Struct. Mol. Biol.*, **14**, 796–806.
14. Hu,Y., Kireev,I., Plutz,M., Ashourian,N. and Belmont,A.S. (2009) Large-scale chromatin structure of inducible genes: transcription on a condensed, linear template. *J. Cell Biol.*, **185**, 87–100.
15. Chowdary,D.R., Dermody,J.J., Jha,K.K. and Ozer,H.L. (1994) Accumulation of p53 in a mutant cell line defective in the ubiquitin pathway. *Mol. Cell. Biol.*, **14**, 1997–2003.
16. Palombella,V.J., Rando,O.J., Goldberg,A.L. and Maniatis,T. (1994) The ubiquitin-proteasome pathway is required for processing the NF-kappa B1 precursor protein and the activation of NF-kappa B. *Cell*, **78**, 773–785.

17. Collins,G.A. and Tansey,W.P. (2006) The proteasome: a utility tool for transcription? *Curr. Opin. Genet. Dev.*, **16**, 197–202.
18. von Mikecz,A. (2006) The nuclear ubiquitin-proteasome system. *J. Cell Sci.*, **119**, 1977–1984.
19. Ferdous,A., Gonzalez,F., Sun,L., Kodadek,T. and Johnston,S.A. (2001) The 19S regulatory particle of the proteasome is required for efficient transcription elongation by RNA polymerase II. *Mol. Cell*, **7**, 981–991.
20. Gonzalez,F., Delahodde,A., Kodadek,T. and Johnston,S.A. (2002) Recruitment of a 19S proteasome subcomplex to an activated promoter. *Science*, **296**, 548–550.
21. Lee,D., Ezhkova,E., Li,B., Pattenden,S.G., Tansey,W.P. and Workman,J.L. (2005) The proteasome regulatory particle alters the SAGA coactivator to enhance its interactions with transcriptional activators. *Cell*, **123**, 423–436.
22. Reid,G., Hubner,M.R., Metivier,R., Brand,H., Denger,S., Manu,D., Beaudouin,J., Ellenberg,J. and Gannon,F. (2003) Cyclic, proteasome mediated turnover of unliganded and liganded ERα on responsive promoters is an integral feature of estrogen signaling. *Mol. Cell*, **11**, 695–707.
23. Stavreva,D.A., Muller,W.G., Hager,G.L., Smith,C.L. and McNally,J.G. (2004) Rapid glucocorticoid receptor exchange at a promoter is coupled to transcription and regulated by chaperones and proteasomes. *Mol. Cell. Biol.*, **24**, 2682–2697.
24. Lipford,J.R., Smith,G.T., Chi,Y. and Deshaies,R.J. (2005) A putative stimulatory role for activator turnover in gene expression. *Nature*, **438**, 113–116.
25. Chi,Y., Huddleston,M.J., Zhang,X., Young,R.A., Annan,R.S., Carr,S.A. and Deshaies,R. (2001) Negative regulation of Gcn4 and Msn2 transcription factors by Srb10 cyclin-dependent kinase. *Genes Dev.*, **15**, 1078–1092.
26. Auld,K.L., Brown,C.R., Casolari,J.M., Komili,S. and Silver,P.A. (2006) Genomic association of the proteasome demonstrates overlapping gene regulatory activity with transcription factor substrates. *Mol. Cell*, **21**, 861–871.
27. Gillette,T.G., Gonzalez,F., Delahodde,A., Johnston,S.A. and Kodadek,T. (2004) Physical and functional association of RNA polymerase II and the proteasome. *Proc. Natl Acad. Sci. USA*, **101**, 5904–5909.
28. Brenner,S. (1974) The genetics of *Caenorhabditis elegans*. *Genetics*, **77**, 71–94.
29. Darzacq,X., Kittur,N., Roy,S., Shav-Tal,Y., Singer,R.H. and Meier,U.T. (2006) Stepwise RNP assembly at the site of H/ACA RNA transcription in human cells. *J. Cell Biol.*, **173**, 207–218.
30. Newton,K., Matsumoto,M.L., Wertz,I.E., Kirkpatrick,D.S., Lill,J.R., Tan,J., Dugger,D., Gordon,N., Sidhu,S.S., Fellouse,F.A. *et al.* (2008) Ubiquitin chain editing revealed by polyubiquitin linkage-specific antibodies. *Cell*, **134**, 668–678.
31. Chen,M., Rockel,T., Steinweger,G., Hemmerich,P., Risch,J. and von Mikecz,A. (2002) Subcellular recruitment of fibrillarin to nucleoplasmic proteasomes: implications for processing of a nucleolar autoantigen. *Mol. Biol. Cell*, **13**, 3576–3587.
32. Boisvert,F.M., Hendzel,M.J. and Bazett-Jones,D.P. (2000) Promyelocytic leukemia (PML) nuclear bodies are protein structures that do not accumulate RNA. *J. Cell Biol.*, **148**, 283–292.
33. Kießlich,A., von Mikecz,A. and Hemmerich,P. (2002) Cell cycle-dependent association of PML bodies with sites of active transcription in nuclei of mammalian cells. *J. Struct. Biol.*, **140**, 167–179.
34. Chartrand,P., Bertrand,E., Singer,R.H. and Long,R.M. (2000) Sensitive and high-resolution detection of RNA in situ. *Methods Enzymol.*, **318**, 493–506.
35. Phair,R.D. and Misteli,T. (2000) High mobility of proteins in the mammalian cell nucleus. *Nature*, **404**, 604–609.
36. Siebrasse,J.P., Grünwald,D. and Kubitscheck,U. (2007) Single-molecule tracking in eukaryotic cell nuclei. *Anal. Bioanal. Chem.*, **387**, 41–44.
37. Siebrasse,J.P., Veith,R., Dobay,A., Leonhardt,H., Daneholt,B. and Kubitscheck,U. (2008) Discontinuous movement of mRNP particles in nucleoplasmic regions devoid of chromatin. *Proc. Natl Acad. Sci. USA*, **105**, 20291–20296.
38. Rockel,T.D., Stuhlmann,D. and von Mikecz,A. (2005) Proteasomes degrade proteins in focal subdomains of the human cell nucleus. *J. Cell Sci.*, **118**, 5231–5242.
39. Axelrod,D., Koppel,D.E., Schlesinger,J., Elson,E. and Webb,W.W. (1976) Mobility measurement by analysis of fluorescence photobleaching recovery kinetics. *Biophys. J.*, **16**, 1055–1069.
40. Kouzarides,T. (2007) Chromatin modifications and their function. *Cell*, **128**, 693–705.
41. Santos-Rosa,H., Schneider,R., Bannister,A.J., Sherriff,J., Bernstein,B.E., Emre,N.C., Schreiber,S.L., Mellor,J. and Kouzarides,T. (2002) Active genes are tri-methylated at K4 of histone H3. *Nature*, **419**, 407–411.
42. Elbi,C., Misteli,T. and Hager,G.L. (2002) Recruitment of dioxin receptor to active transcription sites. *Mol. Biol. Cell*, **13**, 2001–2015.
43. Pombo,A., Jackson,D.A., Hollinshead,M., Wang,Z., Roeder,R.G. and Cook,P.R. (1999) Regional specialization in human nuclei: visualization of discrete sites of transcription by RNA polymerase III. *EMBO J.*, **18**, 2241–2253.
44. Janicki,S.M., Tsukamoto,T., Salghetti,S.E., Tansey,W.P., Sachidanandam,R., Prasanth,K.V., Ried,T., Shav-Tal,Y., Bertrand,E., Singer,R.H. *et al.* (2004) *Cell*, **116**, 683–698.
45. Sirri,V., Urcuqui-Inchima,S., Roussel,P. and Hernandez-Verdun,D. (2008) Nucleolus: the fascinating body. *Histochem. Cell Biol.*, **129**, 13–31.
46. Edgar,L.G., Wolf,N. and Wood,W.B. (1994) Early transcription in *Caenorhabditis elegans* embryos. *Development*, **120**, 443–451.
47. Seydoux,G., Mello,C.C., Pettitt,J., Wood,W.B., Priess,J.R. and Fire,A. (1996) Repression of gene expression in the embryonic germ lineage of *C. elegans*. *Nature*, **382**, 713–716.
48. Baugh,L.R., Hill,A.A., Slonim,D.K., Brown,E.L. and Hunter,C.P. (2003) Composition and dynamics of the *Caenorhabditis elegans* early embryonic transcriptome. *Development*, **130**, 889–900.
49. Seydoux,G. and Dunn,M.A. (1997) Transcriptionally repressed germ cells lack a subpopulation of phosphorylated RNA polymerase II in early embryos of *Caenorhabditis elegans* and *Drosophila melanogaster*. *Development*, **124**, 2191–2201.
50. Lafontaine,D.L. and Tollervey,D. (2000) Synthesis and assembly of the box C+D small nucleolar RNPs. *Mol. Cell. Biol.*, **20**, 2650–2659.
51. Zhao,R., Bodnar,M.S. and Spector,D.L. (2009) Nuclear neighborhoods and gene expression. *Curr. Opin. Genet. Dev.*, **19**, 172–179.
52. Schwartz,A.L. and Ciechanover,A. (2009) Targeting proteins for destruction by the ubiquitin system: implications for human pathobiology. *Annu. Rev. Pharmacol. Toxicol.*, **49**, 73–96.
53. Antón,L.C., Schubert,U., Bacík,I., Princiotta,M.F., Wearsch,P.A., Gibbs,J., Day,P.M., Realini,C., Rechsteiner,M.C., Bennink,J.R. *et al.* (1999) Intracellular localization of proteasomal degradation of a viral antigen. *J. Cell Biol.*, **146**, 113–124.
54. Baldin,V., Militello,M., Thomas,Y., Doucet,C., Fic,W., Boireau,S., Jariel-Encontre,I., Piechaczyk,M., Bertrand,E., Tazi,J. *et al.* (2008) A novel role for PA28gamma-proteasome in nuclear speckle organization and SR protein trafficking. *Mol. Biol. Cell.*, **19**, 1706–1716.
55. Rockel,T.D. and von Mikecz,A. (2002) Proteasome-dependent processing of nuclear proteins is correlated with their subnuclear localization. *J. Struct. Biol.*, **140**, 189–199.
56. Spoel,S.H., Mou,Z., Tada,Y., Spivey,N.W., Genschik,P. and Dong,X. (2009) Proteasome-mediated turnover of the transcription coactivator NPR1 plays dual roles in regulating plant immunity. *Cell*, **137**, 860–872.
57. von Mikecz,A., Chen,M., Rockel,T. and Scharf,A. (2008) The nuclear ubiquitin-proteasome system: visualization of proteasomes, protein aggregates, and proteolysis in the cell nucleus. *Methods Mol. Biol.*, **463**, 191–202.
58. Muratani,M. and Tansey,W.P. (2003) How the ubiquitin–proteasome system controls transcription. *Nat. Rev. Mol. Cell Biol.*, **4**, 192–201.
59. Fátyol,K. and Grummt,I. (2008) Proteasomal ATPases are associated with rDNA: the ubiquitin proteasome system plays a direct role in RNA polymerase I transcription. *Biochim. Biophys. Acta*, **1779**, 850–859.

60. Sikder,D., Johnston,S.A. and Kodadek,T. (2006) Widespread, but non-identical, association of proteasomal 19 and 20S proteins with yeast chromatin. *J. Biol. Chem.*, **281**, 27346–27355.

61. Anindya,R., Aygün,O. and Svejstrup,J.Q. (2007) Damage-induced ubiquitylation of human RNA polymerase II by the ubiquitin ligase Nedd4, but not Cockayne syndrome proteins or BRCA1. *Mol. Cell.*, **28**, 386–397.

62. Harreman,M., Taschner,M., Sigurdsson,S., Anindya,R., Reid,J., Somesh,B., Kong,S.E., Banks,C.A., Conaway,R.C., Conaway,J.W. *et al*. (2009) Distinct ubiquitin ligases act sequentially for RNA polymerase II polyubiquitylation. *Proc. Natl Acad. Sci. USA*, **106**, 20705–20710.

63. Bregman,D.B., Du,L., van der Zee,S. and Warren,S.L. (1995) Transcription dependent redistribution of the large subunit of RNA polymerase II to discrete nuclear domains. *J. Cell Biol.*, **129**, 287–298.

64. von Mikecz,A., Zhang,S., Montminy,M., Tan,E.M. and Hemmerich,P. (2000) CREB-binding protein (CBP)/p300 and RNA polymerase II colocalize in transcriptionally active domains in the nucleus. *J. Cell Biol.*, **150**, 265–273.

65. Xu,Y.X. and Manley,J.L. (2007) Pin1 modulates RNA polymerase II activity during the transcription cycle. *Genes Dev.*, **21**, 2950–2962.

66. Yu,P. and Kodadek,T. (2007) Dynamics of the hypoxia-inducible factor-1-vascular endothelial growth factor promoter complex. *J. Biol. Chem.*, **282**, 35035–35045.